

FOE-NET: Segmentation of Fetal in Ultrasound Images using V-NET

Original Scientific Paper

Eveline Pregitha R.

Research Scholar, Department of Electronics and Communication Engineering,
Noorul Islam Centre for Higher Education,
Tamil Nadu, India
epregitha@gmail.com

Vinod Kumar R. S.

Professor & Head, Department of Electronics and Communication Engineering,
Noorul Islam Centre for Higher Education,
Tamil Nadu, India
rsvinodkumar69@yahoo.co.in

Ebbie Selvakumar C.

Assistant Professor, Department of Electrical and Electronics Engineering,
Rohini College of Engineering and Technology,
Tamil Nadu, India
ebbieve@gmail.com

Abstract – Ultrasound is a non-invasive method to diagnose and treat medical conditions. It is becoming increasingly popular to use portable ultrasound scanning devices to reduce patient wait times and make healthcare more convenient for patients. By using ultrasound imaging, you will be able to obtain images with better quality and also gain information about soft tissues. The interference caused by tissues reflected in ultrasound waves resulted in intensified speckle sound, complicating imaging. In this paper, a novel Foe-Net has been proposed for segmenting the fetal in ultrasound images. Initially, the input US images are noise removal phase using two different filters Adaptive Gaussian Filter (AGF) and Adaptive Bilateral Filter (ABF) used to reduce the noise artifacts. Then, the US images are enhanced using CLAHE and MSR for smoothing to enhance the image quality. Finally, the denoised images are input to the V-net is used to segment the fetal in the US images. The experimental outcomes of the proposed Multi-Scale Retinex (MSR) is an image enhancement technique that improves image quality by adjusting its illumination and enhancing details. Foe-Net was measured by specific parameters such as specificity, precision, and accuracy. The proposed Foe-Net achieves an overall accuracy of 99.48%, specificity of 98.56 %, and precision of 96.82 % for segmented fetal in ultrasound images. The proposed Foe-Net attains better pre-processing outcomes at low error rates and, high SNR, high PSNR, and high SSIM values.

Keywords: Ultrasound images, Adaptive Gaussian Filter, Adaptive Bilateral Filter, CLAHE, Multi-scale retinex, V-net

1. INTRODUCTION

Ultrasound (US) image mechanism is considered an important medical imaging method that is used for visualizing the growth and pathology of the fetus in the womb of a mother. The ultrasound scan sends high-frequency waves through the abdomen into the uterus. This wave gets reflected by the baby and reaches the scanner [1]. Ultrasonic waves are used at frequencies ranging from 2 MHz to 15 MHz Ultrasonic waves reflected by body tissues after traveling through an organ are struck. To create US images, the echoes that reflect are analyzed, and the scattered echoes are referred to

as speckle noise [2]. Speckle noise reduces the clarity and contrast of US images. It is extremely difficult for radiologists to diagnose diseases accurately due to speckle noise. The structural analysis of the US images is distorted by speckle noise [3]. Speckle noise reduces the quality of the images, resulting in low-quality images for the US. Many denoising techniques have been developed to minimize noise, including total variation, wavelet-based filtering techniques, median filtering, nonlocal means, and various other techniques [4].

In recent years, deep learning has been applied to medical image analysis, bringing about a revolutionary impact on the existing diagnostic techniques [5].

US images commonly contain two types of noise due to the technology used to obtain ultrasonic images and the presence of various organs and tissues within the imaging area [6]. The quality and contrast of a US image drastically deteriorate, making medical diagnosis challenging. The Adaptive Gaussian Filter (AGF) is an image analysis method that improves the conventional Gaussian filter by varying its regional visual factors that reduce distortion while maintaining borders and patterns. ABF enhances bilateral filters changing their characteristics to regional image features. The AGF and ABF are more effective compared to different techniques for reducing the level of noise in the original image. CLAHE technique is used for enhancing images to improve spatial brightness and features by breaking an illustration into tiny segments. Histogram equalization [7] is implemented for each segment and limiting contrast enhancement to prevent noise activation. In Multi-scale Retinex (MSR), the illumination and details of an image are adjusted to improve its quality. The CLAHE and MSR are more effective compared to different techniques for enhancing the quality of the original image. The segmentation process simplifies the analysis of images by making them more understandable. When compared to segnet [8], Alexnet [9], and U-Net [10], the proposed V-net achieves better accuracy. As a result, despeckling ultrasound images is critical, and numerous research have been conducted to enhance image quality using noise filtering algorithms and segmentation results.

The main contribution of the research summarised as,

- The main objective of the work is to represent a novel Foe-Net that has been proposed for segmenting the fetal in ultrasound images. Initially, the input US images are noise removal phase using two different filters AGF and ABF used to remove the noise artifacts.
- Then, the US images are enhanced by CLAHE and MSR for smoothing to enhance the image quality. The proposed Foe-Net technique is evaluated based on denoising filters PSNR, MSE, SNR, and SSIM.

The following five divisions were developed for the remaining components of this investigation. The involved works are specified in Section 2, the proposed foe-net is reviewed in Section 3, findings and analysis are reported in Section 4, and a conclusion and recommendations for further study are provided in Section 5.

2. LITERATURE SURVEY

In recent days some methods and techniques remained presented by researchers mainly to detect the fetus efficiently. This section provides a brief overview of the most recent studies.

In 2019 Sobhaninia et al. [11] developed a multitasking deep network for 2D ultrasound image calculation of the fetal head circumference based on a Link-Net ar-

chitecture with multiscale inputs. A completely linked network-based Ellipse Tuner formed part of the organized system.

In 2020 Qiao et al. [12] employed 2D prenatal ultrasound images to propose a DL semantic segmentation network in fetal HC segmentation. A squeeze-and-excitation (SE) block was added to the jump connection, and an advanced convolutional layer was added after the last encoder.

In 2022 Ashkani Chenarlogh et al. [13] developed a novel fast, and accurate U-Net-based architecture for the problem of segmenting medical images. The encoder-decoder path consists of four blocks. Dice and Jaccard coefficients for the dataset using the suggested precise model were 97.62% and 95.43%, respectively.

In 2021 Singh, et al. [14] created an innovative deep-learning method for automatically segmenting the foetal cerebellum from 2D US images. By integrating the residual block (Res), adding extended convolution to the final two slices, and using U-Net as the basis model, able to distinguish the cerebellum (c) from the noisy US image.

In 2023 Cengiz et al. [15] proposed an improved segmentation quality assessment methodology (FUSQA) to automatically classify the quality of a fetal ultrasound segmentation model on unseen data. They contrasted the various designs, attaining over 90% classification accuracy when separating high- and low-quality segmentation masks from a dataset that was unidentified.

In 2022 Cammarasana et al. [16] developed a deep learning system for denoising US pictures in real-time. The most effective method for preserving morphological features and enhancing edges is Weighted Nuclear Norm Minimization (WNNM), which was determined after a comparison of state-of-the-art denoising approaches.

In 2021 Dong et al. [17] a Feature-guided CNN for image denoising using portable ultrasonography equipment was developed. To achieve high-quality denoising outcomes for clinical images, a feature masking layer was utilized to power a tiered denoising system.

From the comprehensive study of the existing works, the observed all existing work has some sort of pitfalls. Therefore, the proposed method focuses on denoising and segmenting the fetal US images using a novel Foe-Net method, a combination of denoising filters and segmenting the US images of fetal.

3. PROPOSED FOE-NET

In this section, a novel Foe-Net for segmenting the fetal in ultrasound images. AGF and ABF are used to remove noise artifacts from US input images. To enhance the quality of the US images, CLAHE and MSR are applied for smoothing. Pre-processed US images are given as input to the deep-learning based V-net for the segmentation of fetal. The overall flow diagram of the proposed method is illustrated in Fig. 1.

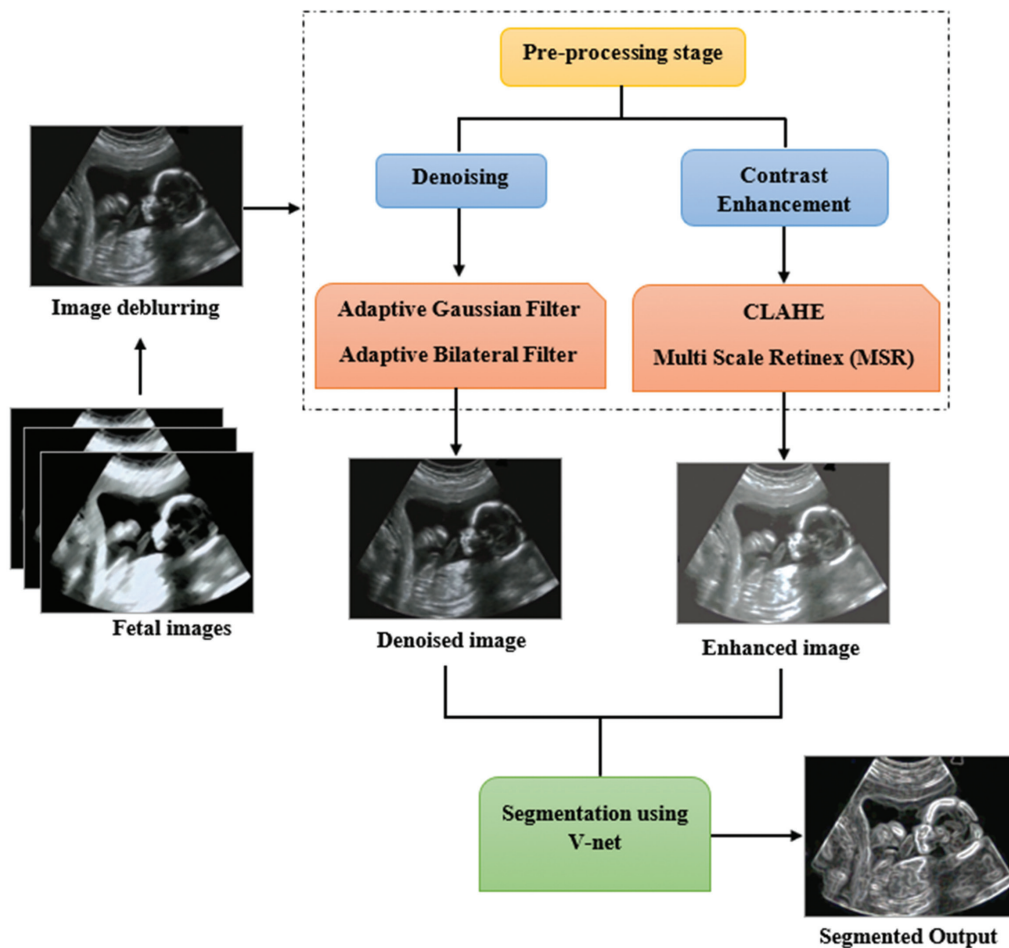


Fig. 1. Schematic representation of proposed methodology

3.1. IMAGE DEBLURRING

Image deblurring techniques have developed recently in response to the pressing demands of numerous businesses for image clarity, and these techniques are currently in use.

If the image destruction process is assumed to be spatially constant, the mathematical method can be expressed in equation (1)

$$f(y,z)=g(y,z)\otimes h(y,z)+m(y,z) \quad (1)$$

It is generally assumed that the process of image degradation is represented by $f(y,z)$ the interaction of spatial motion invariant functions $g(y,z)\otimes h(y,z)$ with additional noise. The following equation (2) can be used to describe the process of image degradation:

$$f(y,z)=G([h(y,z)]+m(y,z)) \quad (2)$$

In the formula from equation (3) the function G is a linear system that satisfies,

$$G[bh_1(y,z)+ch_2(y,z)]=bG[h_1(y,z)]+cG[h_2(y,z)] \quad (3)$$

where b and c are arbitrary values, function G is a linear system, and $h_1(y,z)$ and $h_2(y,z)$ are optional depicts of the same size in equation (4).

$$G[h(y-\alpha, z-\beta)]=f(y-\alpha, z-\beta) \quad (4)$$

The system has space shift invariance $y-\alpha, z-\beta$ at that point, it is typically said in equation (4). It demonstrates

how a point's output is only influenced by its input and not by its geographical position within the system. According to the procedure representation in the frequency domain $F(v,w)$, can be denoted in equation (5)

$$(v,w)=G(v,w)H(v,w)+M(v,w) \quad (5)$$

From the above equation (7) (v,w) the denoted coefficients of the image frequency. The image deblurring approach M is improved and simplified using the below equation (6):

$$F = GH+M \quad (6)$$

The absolute evaluation approach, which is distinguished by evaluation scales by international standards and is the most often applied technique for image deblurring, is immediately categorized based on vision. The results of the evaluation will differ due to the impact of other testers and evaluating situations on image quality, but this method can best capture the impact of image restoration.

3.2. PRE-PROCESSING STAGE

In this phase, the US images are pre-processed in two phases namely denoising using AGF & ABF filtering techniques and enhancement using CLAHE & MSR techniques. Initially, the AGF filter automatically adjusts flattening using localized image features to minimize

distortion while keeping edge patterns in fetal images. Along with suppressing distortion after AGF, the ABF also maintains boundaries by adapting filter variables to localized image qualities. Afterward, the CLAHE effectively improves contrast in images by enhancing the dynamic range of pixel intensity levels. Next, the MSR analyses images at multiple resolutions to eliminate poor illumination and improve the clarity of the image.

3.2.1. Image Denoising

(a) Adaptive Gaussian Filter (AGF)

The image is deformed but the noise is smoothed out when using an adaptive Gaussian filter to reduce the noise. The following terms can be used to express the two-dimensional digital Gaussian filter in equation (7):

$$G(y, z) = \frac{1}{\sqrt{2\pi}\sigma} \exp\left(-\frac{y^2+z^2}{2\sigma^2}\right), \quad (7)$$

Where σ^2 is the Gaussian filter's variance, and the size of the filter kernel $k(-k \leq y, z \leq k)$ is frequently calculated by excluding values that are smaller than the kernel's maximum value. The expression for the one-dimensional Gaussian filter $G(y)$ is denoted in equation (8),

$$G(y) = \frac{1}{\sqrt{2\pi}\sigma} \exp\left(-\frac{y^2}{2\sigma^2}\right) \quad (8)$$

When the Gaussian filter is used to reduce noise, a high filter variance is successful at reducing noise, but it also distorts the areas of the image where there are sharp fluctuations in pixel brightness. The adaptive filter variance $\sigma^2(y)$ is defined in equation (9):

$$\sigma^2(y) = \frac{2\varepsilon}{|E''(y)|}, \quad (9)$$

Where ε is the step of predefined error brought on by a Gaussian filter. $E''(x)$ is determined using a complex regression-based method from the noisy, distorted signal.

The goal of the adaptive Gaussian filtering problem is to minimize the mean square error while ensuring that the filter variance does not significantly shift from pixel to pixel. Let G and E stand for the image and the two-dimensional Gaussian filter, respectively.

(b) Adaptive Bilateral Filter (ABF)

For removing noise artifacts, images are pre-processed using adaptive bilateral filters. The adaptive bilateral filter is a new sharpening and smoothing technique (ABF). Where $[x_t, y_t]$ and Ω_{x_t, y_t} are defined as before, and the normalization factor, the suggested shift-variant ABF's response at $[x_t, y_t]$ to an impulse at $[x, y]$ at the bottom is given by equation (10),

$$r_{x_t, y_t} = \sum_{x=x_t-M}^{x_t+M} \sum_{y=y_t-M}^{y_t+M} \exp\left(-\frac{(x-x_t)^2+(y-y_t)^2}{2\sigma_d^2}\right) \times \exp\left(-\frac{(f[x, y]-f[x_t, y_t]-\zeta[x_t, y_t])^2}{2\sigma_r^2[x_t, y_t]}\right) \quad (10)$$

ABF includes two significant modifications but maintains the basic structure of a bilateral filter. ABF is first given an offset ζ . Second, the ABF's locally adaptable parameters include both the width and ζ of the range filter.

ABF is a fixed low-pass Gaussian domain filter. If $f=0$ and r is fixed, the ABF transforms into a normal bilateral filter (BL). The domain filter of the ABF is a fixed low-pass Gaussian filter. The BL smooths and sharpens when combined with a locally adaptive ζ and σ_r . Let Ω_{x_t, y_t} denote the group of pixels in the window of pixels $(2M+1) \times (2M+1)$ centered at $[x_t, y_t]$.

The initial threshold value is calculated by using the following equation (11) and considering the brightness d_u and d_v of pixels e_i and e_j

$$SB = Z \times \sum_{e=0}^{255} \frac{d_u+d_v}{2} \quad (11)$$

where Z stands for the Laplacian second-order differential equation used to isotopically distribute pixels across the blood smear images. The equation (12) is to calculate Z .

$$Z = \frac{\partial^2 Z}{\partial e_i} + \frac{\partial^2 Z}{\partial e_j} \quad (12)$$

The pre-processed image has been blurred, the edges may not have been retained, and the image will look flattened even though the pre-processing is complete and the image is noise-free.

3.2.2. Image Enhancement

(a) CLAHE

CLAHE improves adaptive histogram equalization. The image appears more natural due to the limitation on the amplification of noise in the image, which overcomes the problems possessed by AHE. In addition to producing an optimal equalization, it seems to be an effective algorithm for obtaining a good-quality ultrasound fetal image. It raises the brightness level to a particular range, making it easier to compare various portions of an image. CLAHE works by partitioning the image into many nonoverlapping regions that have almost equal sizes and HE is applied to each one. The CLAHE filter method was primarily created for medical imaging, and it aims to reduce the noise produced by homogeneous areas. When pre-processing digital photos, the procedure can be used to improve the image by removing noise. Rather, than using the complete image, CLAHE works on discrete areas of the image called tiles. CLAHE is an improved form of HE (Histogram Equalization), a quick and efficient technique for enhancing images that can improve the contrast by reducing the grayscale. If colored images are utilized, the input images are greyed out and CLAHE suggests the three channels. The effects of CLAHE processing on images are in Fig. 2.

(b) MSR

The MSR technique is used for pre-processing, which has become more popular in recent years. It is commonly known as MSR for enhancing fetal ultrasound images. Numerous researchers have developed a variety of Retinex-based image enhancement algorithms, including the single-scale Retinex algorithm, multi-scale Retinex algorithm, and multi-scale Retinex algorithm with colour restoration.

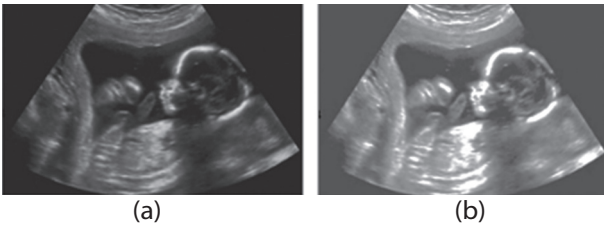


Fig. 2. (a) Original image, and (b) Image enhanced using CLAHE

Then, averaging and adding the results of the filtering on different scales can maintain the image's high quality, reduce its dynamic range, and achieve colour improvement and consistency. The algorithm of the Multi-Scale Retinex (MSR) is as follow in equation (13) and (14):

$$S(j) = R_v(j) \cdot \sum_{m=1}^M \omega_m \{ \log Y(j) - \log [g(j) \otimes Y(j)] \} \quad (13)$$

$$R_v(j) = \beta \{ \log [\alpha Y(j)] - \log [\sum_{j=1}^n Y(j)] \} \quad (14)$$

R_v stands for the color parameter of the v -th channel, which is used to modify the ratio of the color of the three channels, where $S(j)$ is enhanced output for MSR, $Y(j)$ is the input image, and $g(j)$ is the filter function, β is a gain contrast and α controls the nonlinear strength, $n = 3$ represents the three channels of RGB.

3.3. V-NET

The V-net network framework contains encoders and decoders. V-Net is an advanced neural network designed for efficient image segmentation in medical images. V-Net is useful for complex frameworks and 3D medical images. Additionally, it reduces fading gradients problems enhances training reliability, and enables more modern performance in segmentation than other traditional networks. The encoder comprised numerous phases, each of which had a different resolution. Finally, after a long decompression process, the decoder can provide an output image with the same size as the original image. Additionally, V Net uses Res Net's short-circuit connection method to learn the residual function simultaneously like every phase's input and output. When waiting, the cross-entropy loss function is replaced with the dice reduction rate to increase the susceptibility of the desired segment area. used a V Net network where the encoder part extracted global features of the decoder component and generated a full-resolution result from the source visual. It is suggested that the V net's fundamental structure is for segmenting fetal tissue. The architecture diagram of the V net is shown in Fig. 3.

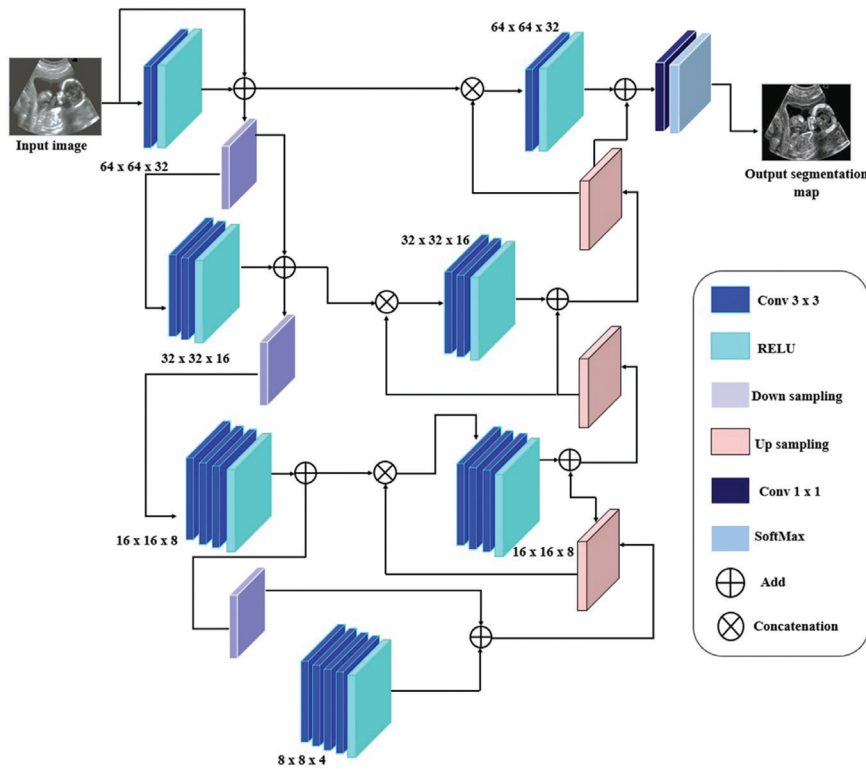


Fig. 3. V-net architecture

Fig. 3 displays the structure of V-Net, which holds the properties of the encoder/decoder structure. The entire network consists of convolutional blocks, non-convolutional blocks, and a final layer of convolutional outputs. Each convolution block consists of 32 convolution kernels, 32 regularization functions, and 32 ReLU activation functions.

These convolution blocks extract features using the convolution kernel's 4, 8, 16, 32, and 64 channels while reaching phase 1. Compression is employed to reduce the quantity of memory needed during training by replacing the pooling process in the down-sampled phase with a kernel of convolution and a variable duration overlap.

The size of the output feature map matches the input and is determined by a remnant pooling engine that includes pooling layers, convolution layers, and remnant structures. Then a suitable stage is inserted, followed by the data supplied for the following level. To create a photo with the exact size as the data input, the last layer of convolution applies an efficient convolution base. It is a widely used loss function in the field of medical image segmentation and is perfect for balancing backdrop and background information.

4. RESULT AND DISCUSSION

In this section, the efficiency of the Proposed Foe-Net is estimated using Matlab-2019b. This work was evaluated and compared with a database of 100 fetal images from subjects between 6 and 20 weeks of maturation. The database images were collected using a variety of scanning techniques, including the THI

Siemens machine, the Wipro GE Logic 400, the Toshiba color Doppler tests, and others. There are 100 images gathered from different ultrasound institutions in the Kanyakumari District of Tamil Nadu, India. This dataset consisted of 80% training images, 10% testing images, and 10% validation images. The performance of the Proposed Foe-Net is estimated through the validation of denoising metrics like MSE, SNR, SSIM, and PSNR of standard processing metrics. The competence of the proposed Foe-Net is assessed by the SSIM, PSNR, and MSE. The PSNR is a frequently used metric to determine the image quality and SSIM is utilized to measure the similarity value between the ground truth and the produced output of the proposed network. There is a comprehensive comparison between the reference and altered images. MSE is a measure of the error ratio between the original and inpainted images. MSE values are used to evaluate the effectiveness of a model with a lower error rate considered more effective. The evaluation of the parameters is given below,

Data analysis results show the effectiveness of this method using maximum PSNR and SSIM in equation (15).

$$PSNR = 10 \cdot \log_{10} \left(\frac{MAX_I^2}{MSE} \right) \quad (15)$$

The ratio of signal power to background noise is called the SNR. It is explained in equation (16).

$$SNR = \frac{D_s}{\hat{\sigma}_m} \quad (16)$$

Where D_s is the estimated image signal density and $\hat{\sigma}_m$ is the estimated image noise standard deviation.

Mean Squared Error (MSE) is a measure of the total squared error between the denoised image and the raw image. It is calculated in equation (17):

$$MSE = \sum_{U,V} \frac{[m_1(u,v) - m_2(u,v)]^2}{U \cdot V} \quad (17)$$

where the dimensions of the image are U and V and $m_1(u, v)$ is the original image. $m_2(u, v)$ is an approximate version of the filtered image.

The SSIM measures the structural similarity between the original and denoised images. It's described as equation (18):

$$SSIM(y, z) = \frac{(2\mu_y\mu_z + a_1)(\sigma_{yz} + a_2)}{(\mu_y^2 + \mu_z^2 + a_1)(\sigma_y^2 + \sigma_z^2 + a_2)} \quad (18)$$

where, μ_y and μ_z the average values and, σ_y and σ_z are the image's standard deviations.

The dice index (DI) uses both a reproducibility validation metric and an index of spatial overlap of the fetal images. DI is calculated to determine the exact ratio of the true region (fetal) to pixels. The predicted fetal pixels and background pixels are calculated in equation (19). Jaccard index (JI) measures the similarity between two finite samples by dividing intersection sizes by union sizes. JI is determined which measures the similarity between actual fetal pixels and predicted fetal pixels.

$$DI = \frac{2T_{pos}}{F_{pos} + 2T_{pos} + F_{neg}} \quad (19)$$

$$JI = \frac{T_{pos}}{T_{pos} + F_{neg} + F_{pos}} \quad (20)$$

Where T_{pos} and T_{neg} means true positives and negatives of the sample images, F_{pos} and F_{neg} specifies false positives and negatives of the sample images. The performance analyzed by these metrics is shown in Table.1.

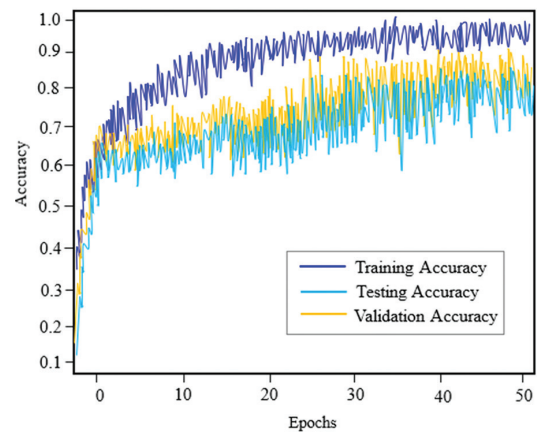


Fig 4. Training and testing accuracy of the proposed method

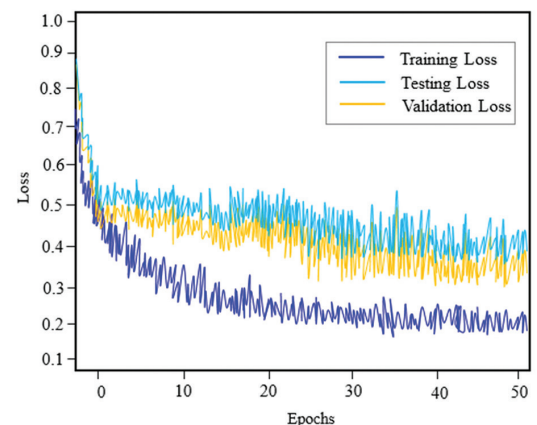


Fig 5. Training and testing loss of proposed method

Figs. 4 and 5 show the results of 100 completed training epochs that were used to test the accuracy and loss of the model. Additionally, the test dataset utilized for each of these techniques was filled with images that were collected from the dataset. Epochs and accuracy for the suggested strategy are correlated in Fig. 4. It is evident that when the epoch value is raised, the model's performance improves. The epochs and loss curves in Fig. 5 show that the model loss will decrease as the number of epochs increases. Therefore, the proposed model was highly reliable for the accurate prediction of fetal in ultrasound images.

The denoised output of the pre-processing filters is shown in Fig. 6

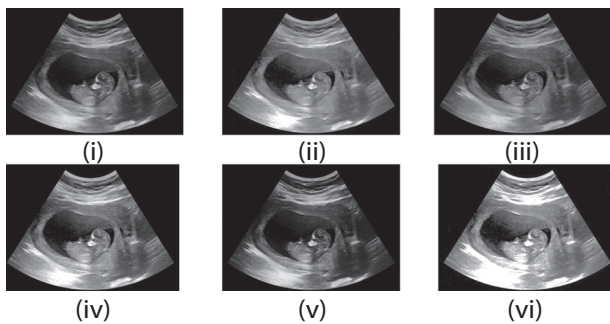


Fig. 6. Denoised output of the pre-processing filters: (i) Original image, (ii) Median filter, (iii) gaussian filter, (iv) bilateral filter, (v) wiener filter, and (vi) Proposed AGF and ABF filters

Fig. 6 expresses the denoised images produced by the pre-processing filters. The fetal input image from the acquired dataset is displayed in section (i). The median filter classified image is shown in section (ii), the Gaussian filter noise reduction images are shown in portion (iii), the bilateral filter pre-processed image is shown in section (iv), the wiener filter enhanced image is shown in portion (v), and the proposed AGF and ABF filter image is demonstrated in portion (vi).

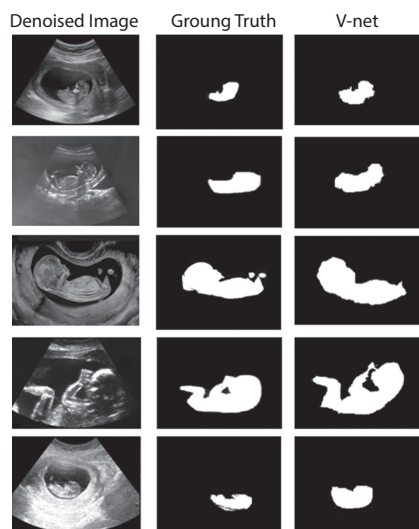


Fig. 7. The experimental segmented results of the proposed model

Fig. 7 shows the results of the proposed Foe-Net obtained from the dataset. Denoising the input fetal images using AGF and ABF filters followed by CLAHE and MSR filters are applied to enhance the quality of images as depicted in column 1. The segmented ground truth images are shown in column 2. Then, the V-net approach for segmenting the input images in column 3. The segmentation result reveals (Fig. 7) that the V-net performs faster and attains the best results based on the Jaccard index and dice index.

Table 1. Performance evaluation of the proposed method using denoising metrics

AUTHOR	METHODS	ACCURACY
Sobhaninia et al. [11]	Link-Net	88.96%
Ashkani Chenarlogh et al. [13]	U-Net	97.62%
Cengiz et al. [1]	FUSQA	90%
Proposed method	Foe-Net	99.48%

Table 1 shows the performance analysis of different image de-noising techniques such as median filter, gaussian filter, and bilateral filter. The proposed Foe-Net achieves MSE values of 0.28, 0.36, and 0.26 for noise rates of 1%, 3% and 5%, respectively. The proposed Foe-Net achieves SSIM values of 0.65, 0.66, and 0.58 for signal-to-noise ratios of 1%, 3%, and 5%, respectively. The proposed Foe-Net achieves SNR values of 32.53, 28.17, and 32.14 at signal-to-noise ratios of 1%, 3%, and 5%, respectively. Then the proposed Foe-Net obtains PSNR values of 68.52, 73.52, and 73.48 for noise rates of 1%, 3%, and 5%, respectively. From the analysis, the proposed Foe-Net gives the minimum MSE, PSNR, SNR, and SSIM compared to other denoising techniques.

4.2. COMPARATIVE ANALYSIS

The comparative analysis section analyzes the performance of existing and proposed models. Table 2 shows the comparison of existing deep learning networks and the proposed Foe-Net for segmenting the fetal in ultrasound images. The accuracy achieved by the proposed Foe-Net is 99.48%, which is better than the accuracy of existing deep learning networks. The proposed method performance is compared with the different deep learning networks such as Ghost Net, AlexNet, and U-net.

Table 2. Comparison of different deep learning networks

Networks	Accuracy	Specificity	Precision	Jaccard index	Dice index
Ghost Net [21]	95.48	94.34	93.26	94.32	81.74
Alex Net [22]	96.32	95.59	94.27	90.48	80.53
U-net [23]	98.46	96.18	95.08	89.51	78.73
V-net	99.48	98.56	96.82	96.67	85.82

From Table 2., the comparison was made between various segmentation algorithms in terms of the performance metrics. The segmentation performance is evaluated in terms of the accuracy, precision, specificity, recall, f1 score, dice score, and Jaccard index as shown in table.2. The V-net increases the overall Jaccard index by 2.43%, 6.84%, and 7.40% better than Ghost Net [21], Alex Net [22], and U-net [23] respectively. The V-net increases the overall Dice index by 4.75%, 6.16%, and 8.26% better than Ghost Net [21], Alex Net [22], and U-net [23] respectively. However, the classic segmentation networks did not perform well compared to the V-net.

Table 3. The comparison between the proposed Foe-Net and state-of-the-art models

Noise Ratio	Performance Metrics	De-noising techniques			
		Median filter [18]	Gaussian filter [19]	Bilateral filter [20]	Proposed
1%	PSNR	43.25	38.16	54.24	68.52
	MSE	0.72	0.56	0.43	0.28
	SSIM	0.26	0.43	0.56	0.65
	SNR	11.04	19.54	24.68	32.53
3%	PSNR	50.64	56.25	64.28	73.52
	MSE	0.86	0.63	0.59	0.36
	SSIM	0.46	0.57	0.64	0.66
	SNR	14.3	20.62	25.06	28.17
5%	PSNR	49.42	58.79	67.81	73.48
	MSE	0.68	0.45	0.38	0.26
	SSIM	0.24	0.34	0.43	0.58
	SNR	24.7	28.61	30.5	32.14

Table 3 demonstrates how our novel network works better than the earlier methods. Several metrics are used to compare existing models with high classification accuracy. In comparison to Link-Net, U-Net, and FUSQA the Proposed Foe-Net increases overall accuracy by 10.5%, 1.90%, and 9.52%, respectively. The proposed Foe-Net results are therefore particularly trustworthy for glaucoma identification.

5. CONCLUSION

This paper proposed a novel Foe-Net for segmenting the fetal in ultrasound images. Initially, the input US images are noise removal phase using two different filters AGF and ABF, to reduce the noise artifacts. Then, the US images are enhanced using CLAHE and MSR for smoothing to enhance the quality of the image. The efficiency of the proposed Foe-Net was evaluated through the validation of denoising metrics like MSE, SNR, SSIM, and PSNR. The proposed Foe-Net gives an overall accuracy of 99.48% achieved for segmented fetal in ultrasound images. In comparison to Link-Net, U-Net, and FUSQA the Proposed Foe-Net increases overall accuracy by 10.5%, 1.90%, and 9.52%, respectively. The proposed Foe-Net achieves MSE values of 0.28, 0.36, and 0.26 for noise rates of 1%, 3% and 5%, respectively.

The experimental outcomes show the PSNR, MSE, SNR, and SSIM of the proposed method which is significant compared to other techniques. In future research, the network performance will be examined using greater data sets directly from several fetal individuals. In addition, we'll look for and categorize structural deviations in the fetal heart.

6. ACKNOWLEDGMENT

The author would like to express his heartfelt gratitude to the supervisor for his guidance and unwavering support during this research for his guidance and support.

7. REFERENCES:

- [1] K. Niha, S. Amutha, B. Surendiran, "Deep Learning Techniques for Foetal and Infant Data Processing in a Medical Context", Healthcare Industry, Vol. 4, 2023, pp. 19-50.
- [2] A. Jegatheesh, N. Kopperundevi, M. A. Sahaya Infant Tinu, "Brain aneurysm detection via firefly optimized spiking neural network", International Journal of Current Bio-Medical Engineering, Vol. 01, No. 01, 2023, pp. 23-29.
- [3] R. Ren, Z. Guo, Z. Jia, J. Yang, N. K. Kasabov, C. Li, "Speckle noise removal in image-based detection of refractive index changes in porous silicon microarrays", Scientific Reports, Vol. 9, No. 1, 2019, p. 15001.
- [4] A. Nithya, A. Appathurai, N. Venkatadri, D. R. Ramji, C. A. Palagan, "Kidney disease detection and segmentation using artificial neural network and multi-kernel k-means clustering for ultrasound images", Measurement, Vol. 149, No. 106952, 2020, p. 40.
- [5] E. Fenil, G. Manogaran, G. N. Vivekananda, T. Thanjaivadivel, S. Jeeva, "Real time violence detection framework for football stadium comprising of big data analysis and deep learning through bidirectional LSTM", Computer Networks, Vol. 151, 2019, pp. 191-200.
- [6] P. G. Sreelekshmi, P. L. Babu, P. J. Shermila, "Leukemia classification using a fusion of transfer learning and support vector machine", International Journal of Current Bio-Medical Engineering, Vol. 1, No. 1, 2023, pp. 1-8.
- [7] Dakshina, D. R. Valiaveetil, A. Bindhu, "Alzheimer disease detection via deep learning-based shuffle network", International Journal of Current Bio-Medical Engineering, Vol. 1, No. 1, 2023, pp. 9-15.

- [8] A. Saood, I. Hatem, "COVID-19 lung CT image segmentation using deep learning methods: U-Net versus SegNet", *BMC Medical Imaging*, Vol. 21, No. 1, 2021, pp. 1-10.
- [9] K. Rasheed, F. Junejo, A. Malik, M. Saqib, "Automated fetal head classification and segmentation using ultrasound video", *IEEE Access*, Vol. 9, 2021, pp. 160249-160267.
- [10] M. Amiri, R. Brooks, H. Rivaz, "Fine-tuning U-Net for ultrasound image segmentation: different layers, different outcomes", *IEEE Transactions on Ultrasonics, Ferroelectrics, and Frequency Control*, Vol. 67, No. 12, 2020, pp. 2510-2518.
- [11] Z. Sobhaninia, S. Rafiei, A. Emami, N. Karimi, K. Najarian, S. Samavi, S. R. Soroushmehr, "Fetal ultrasound image segmentation for measuring biometric parameters using multi-task deep learning", *Proceedings of the 41st Annual International Conference of the IEEE Engineering in Medicine and Biology Society*, Berlin, Germany, 23-27 July 2019, pp. 6545-6548.
- [12] D. Qiao, F. Zulkernine, "Dilated squeeze-and-excitation U-Net for fetal ultrasound image segmentation", *Proceedings of the IEEE Conference on Computational Intelligence in Bioinformatics and Computational Biology*, Via del Mar, Chile, 27-29 October 2020, pp. 1-7.
- [13] V. A. Chenarlogh, M. G. Oghli, A. Shabanzadeh, N. Sirjani, A. Akhavan, I. Shiri, H. Arabi, M. S. Taheri, M. K. Tarzamni, "Fast and accurate U-net model for fetal ultrasound image segmentation", *Ultrasonic Imaging*, Vol. 44, No. 1, 2022, pp. 25-38.
- [14] V. Singh, P. Sridar, J. Kim, R. Nanan, N. Poornima, S. Priya, G. S. Reddy, S. Chandrasekaran R. Krishnakumar, "Semantic segmentation of cerebellum in 2D fetal ultrasound brain images using convolutional neural networks", *IEEE Access*, Vol. 9, 2021, pp. 85864-85873.
- [15] S. Cengiz, I. Almakk, M. Yaqub, "FUSQA: Fetal Ultrasound Segmentation Quality Assessment", arXiv:2303.04418, 2023.
- [16] S. Cammarasana, P. Nicolardi, G. Patanè, "Real-time denoising of ultrasound images based on deep learning", *Medical & Biological Engineering & Computing*, Vol. 60, No. 8, 2022, pp. 2229-2244.
- [17] G. Dong, Y. Ma, A. Basu, "Feature-guided CNN for denoising images from portable ultrasound devices", *IEEE Access*, Vol. 9, 2021, pp. 28272-28281.
- [18] G. Yang, W. Feng, J. Jin, Q. Lei, X. Li, G. Gui, W. Wang, "Face mask recognition system with YOLOV5 based on image recognition", *Proceedings of the IEEE 6th International Conference on Computer and Communications*, Chengdu, China, 11-14 December 2020, pp. 1398-1404.
- [19] K. M. Jaeger, M. Nissen, R. Richer, S. Rahm, A. Titzmann, P. A. Fasching, B. M. Eskofier, H. Leutheuser, "Machine Learning-based Detection of In-Utero Fetal Presentation from Non-Invasive Fetal ECG", *Proceedings of the IEEE-EMBS International Conference on Biomedical and Health Informatics*, Ioannina, Greece, 27-30 September 2022, pp. 1-4.
- [20] M. Elhoseny, K. Shankar, "Optimal bilateral filter and convolutional neural network based denoising method of medical image measurements", *Measurement*, Vol. 143, 2019, pp. 125-135.
- [21] I.A. Kazerouni, G. Dooly, D. Toal, "Ghost-UNet: an asymmetric encoder-decoder architecture for semantic segmentation from scratch", *IEEE Access*, Vol. 9, 2021, pp. 97457-97465.
- [22] S. Lu, Z. Lu, Y. D. Zhang, "Pathological brain detection based on AlexNet and transfer learning", *Journal of computational science*, Vol. 30, 2019, pp. 41-47.
- [23] X. X. Yin, L. Sun, Y. Fu, R. Lu, Y. Zhang, "U-Net-Based medical image segmentation", *Journal of Healthcare Engineering*, Vol. 2022, 2022.